ENGINEER - Vol. LVI, No. 02, pp. [23-35], 2023

DOI: https://doi.org/10.4038/engineer.v56i2.7574

Three-Dimensional Numerical Simulation for Lateral Distortional Buckling Behaviour of Steel-Concrete Composite Beams

W.M.A.D. Wijethunge, A.J. Dammika, C.S. Bandara and J.A.S.C. Jayasinghe

Abstract: Lateral Distortional Buckling (LDB) is a mode of instability in Steel-Concrete Composite (SCC) beams that is yet to be fully understood by the structural engineering research and design community. This work investigated numerical methods to understand the LDB behavior of SCC beams under negative moments that exhibit nonlinear behavior. Focus of the study was to develop and validate 3-Dimensional finite element (FE) models which capture the LDB behavior of SCC beams precisely. Detailed 3-Dimensional FE models of the SCC beams were developed using ABAQUS. For modeling concrete, a nonlinear damage plasticity model was considered. A quad-linear curve was used to describe the stress-stain relationship for the steel beam. The stress-stain relationship for the rebar was described using a bi-linear curve while an elastic perfectly plastic model was assigned to the headed stud shear connectors. Steel hardening behavior was simulated using an isotropic hardening model. The interaction between the concrete slab, steel beam, and studs was described using appropriate interface elements combined under suitable constraints. The FE model's accuracy was validated by results obtained from previous experiments found in literature together with a brief description of the experiments done by previous researchers to ensure completeness. Validation of the model was done by comparing Moment-Rotation curves obtained from the experimental tests, lateral displacements of the bottom flange along the axial direction and comparison of the failure modes between the numerical model and experimental test specimens. It was observed that the maximum relative error for the ultimate moment capacity of the composite beams from FE analysis and the experimental tests was less than 2% which shows that the FE model was in strong agreement with the experimental results. Accordingly, the numerical model developed herein proves to be capable of accurately representing the LDB phenomenon.

Keywords: Steel-concrete composite beam, Lateral distortional buckling, Negative moment, Nonlinear FE analysis

1. Introduction

Steel-Concrete Composite (SCC) beams are a form of beams that efficiently utilizes the characteristics of both concrete and steel materials. SCC beams comprise concrete slabs resting upon steel beams, bonded together by shear connectors to prevent separation or relative slip between the concrete slab and the steel beam [1]. Shear connectors in composite beams play the vital role of transferring longitudinal shear stresses at the interface between the steel beam and the concrete slab allowing composite beam behaviour [2]. These composite structural members are widely used in construction industry due to their advantages such as the reduced section depth, savings in steel weight, rapid constructability, and elimination of formwork. Furthermore, the concrete slab may protect the steel against fire and corrosion as well. Behaving as a single composite section enhances the structural efficiency.

*Eng. (Ms.) **W.M.A.D. Wijethunge,** AMIE (SL), BTech Hons (Eng) (OUSL), Research Assistant, Department of Civil Engineering, Faculty of Engineering, University of Peradeniya.*
Email:akilawijethunge@gmail.com
https://orcid.org/0000-0002-0138-4427
*Eng. (Dr.) **A.J. Dammika,** AMIE(SL), B.Sc.Eng. (Peradeniya), M.Eng. (AIT), PhD. (Saitama), Senior Lecturer, Department of Civil Engineering, Faculty of Engineering, University of Peradeniya.*
Email:dammikaaaj@gmail.com
https://orcid.org/0000-0002-2587-3743
*Eng. (Dr.) **C.S. Bandara,** C.Eng., MIE(SL), B.Sc.Eng. (Peradeniya), M.Sc.Eng. (Peradeniya), PhD. (Peradeniya), Senior Lecturer, Department of Civil Engineering, Faculty of Engineering, University of Peradeniya.*
Email:csbandara@eng.pdn.ac.lk
http://orcid.org/0000-0003-4141-8983
*Eng. (Dr.) **J.A.S.C. Jayasinghe,** AMIE (SL), B.Sc.Eng. (Peradeniya), M.Eng. (AIT), PhD. (Tokyo), Senior Lecturer, Department of Civil Engineering, Faculty of Engineering, University of Peradeniya.*
Email:supunj@pdn.ac.lk
http://orcid.org/0000-0003-1054-9358

Composite structural systems are well recognized in terms of stiffness and strength compared to non-composite solutions [3], [4]. It is possible to utilize the advantages from both materials by having a steel beam (to withstand tensile stresses) and a concrete slab (to withstand compressive stresses) [5]. This combination allows higher stiffness and smaller structural sections. As a result, the concrete slab is in compression and the steel beamis in tension.

However, in building construction, the use of rigid and semi-rigid connections is common, resulting in negative moments in the beams, tensile stresses in the concrete slab, and compressive stresses in the steel beam. In instances where sufficient lateral restraint is not provided, compressive stresses in the bottom flange of the steel section can cause lateral instability with web distortion, referred to as Lateral Distortional Buckling (LDB) [6], [7].

LDB is defined as lateral displacement accompanied by the rotation of compressed bottom flange caused by web distortion (Figure 1(a)) when the web is not rigid enough to withstand lateral flexion [6]. Web distortion effect is not considered in the Lateral Torsional Buckling (LTB) phenomenon and it is assumed that, during buckling, a given cross-section moves laterally within its own plane and twists as a rigid body (Figure(1b)) [8]. The Vlasov's assumption ignores possible distortional deformations of the web within the plane of the cross-section (Figure 1(a)), resulting in an overestimation of the lateral torsional buckling capacity [6].

While distortional effects may be minor in some cases, previous research has demonstrated that distortional effects become more significant in beams with slender webs, stocky flanges, and/or shorter spans. In such cases, omitting web distortion leads to an overestimation of the member's lateral torsional buckling capacity [9]. LDB is possible to occur whenever the tension flange is completely restrained against lateral deformation and twist, in instances like half-through girder bridges, SCC beams and beams on seat supports. It may also occur when a concentrated load acts on the restrained compression flange (Figure 2) [9].

The studies on LDB in SCC beams are concentrated on analysing the elastic behaviour of LDB to develop a method for determining the elastic critical moment or on analysing the LDB strength.

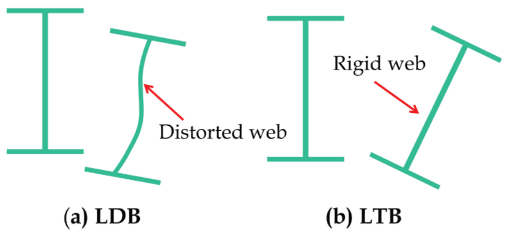

Figure 1 – LDB and LTB Buckling Modes of I-Beams

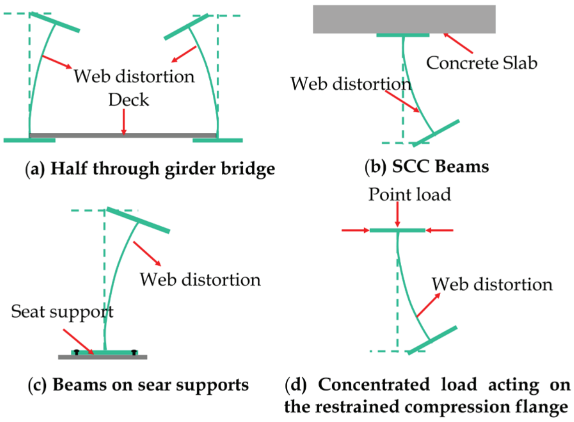

Figure 2 – Possible Instances where LDB can Occur

However, there appears to be no consensus in the proposed methodologies, as divergences are observed in the determination of the elastic critical moment compared to numerical analysis results [10]. Furthermore, the methodologies proposed in various works for estimating the elastic critical moment can result in the inaccurate determination of the strength of SCC beams under negative moments by standard procedures. Another area to consider is the verification of divergence between the ultimate moment results obtained through experimental tests or numerical analyses and the procedures outlined in standard codes of practice [6].

It is widely known that laboratory tests are time-consuming, expensive and in some cases, unfeasible. However, in recent years, Finite Element Analysis (FEA) has become an effective and useful tool for analysing a wide range of engineering problems. According to Abdollahi [11], a comprehensive FE model allows for a significant reduction in the number of experiments conducted. However, for a thorough investigation of any structural system, the experimental phase must be conducted.

When studying a specific structural phenomenon, numerical models must be correlated to reliable experimental results, to ensure that experimental and numerical analysis are in agreement.

This paper focuses on developing realistic 3-dimensional FE models which simulate the LDB behaviour of SCC beams that agrees with experimental results of two SCC beams tested by Tong et al. [12]. The two SCC beams are different in degree of shear connections. A brief description of the experiment conducted by Tong et al. [12] is explained and ABAQUS is used to conduct nonlinear analysis that includes both material and geometrical nonlinearity. Refined numerical models were created by considering several effects, including the initial geometric imperfection, residual stresses, shear connectors and material nonlinearity. The numerical results obtained through FEM were validated by using responses measured from the experiments conducted by Tong et al. [12]. This was done by comparing the Moment-Rotation curves of SCC beams, moment capacity of beams, lateral displacement of the bottom flange along the axial direction and the failure modes between the numerical models and experimental test specimens.

2. Literature Review

Experimental studies of local buckling and LDB on composite beams in a region of negative moment are less common, reportedly because they are expensive and difficult to carry out [13]. Furthermore, according to Rossi et al. [6] and Bradford and Kemp [13], the recommendations of the standard codes such as British standards (BS5400:1985), Eurocode 4 (EN 1994-1-1-2004), Australian standards (AS/NZS 2327 and AS4100), North American standards (AISC 360-2016 and AASHTO 2017) and Brazilian standards (ABNT NBR 8800:2008) in this context are imprecise. On the other hand, the development of numerical analyses capable of accommodating a variety of effects such as initial geometric imperfection, residual stresses, and slippage between the concrete and steel interfaces, geometric nonlinearity, and material nonlinearity, has increased the feasibility of investigating composite structures.

Chen and Jia [7] presented a numerical study that investigated the occurrence of LDB in SCC beams. Purpose of this ABAQUS based analysis was to investigate the LDB strength of prestressed composite beams. It was discovered that the LDB strength decreases with increasing prestressing force and that the web slenderness and compressed flange slenderness have a significant influence on the LDB strength. Vasdravellis et al. [5] investigated the effects of negative moment action and axial compression load in combination. It was found that when a compressive load acts on the composite section, the strength to the negative moment is significantly reduced and the local buckling in the steel beam is more significant, affecting the section's ductility.

Chen and Wang [14] also investigated the influence of web stiffeners on the LDB strength of SCC beams using nonlinear numerical analyses. It was discovered that the use of web stiffeners significantly increases the strength of composite beams under the action of negative moment, and that the Eurocode 4 standard procedure yields conservative LDB strength results. It is generally known that, in practice, web stiffeners are added to steel I-beams if the web buckling criteria are not satisfied. This could potentially reduce the LDB effect. However, there are limitations in the present design procedures. Furthermore, currently there is no general design method to assess the contribution of transverse web stiffeners to the strength of SCC beams [14]. Therefore, the added web stiffeners may not be sufficient to resist the LDB effect. Hence, there is a need of deciding on an optimal web stiffener configuration that would minimize the LDB effect while satisfying the web buckling criteria.

Liu and Sun [15] also developed FE models under negative moments to study the LDB behaviour. This study demonstrated that the FE method is versatile and effective for analysing the mechanical behaviour of composite beams subjected to negative bending. Subsequently, Zhou and Yan [16] used the ANSYS software to validate the SCC beams developed by Tong et al. [12]. After validating the numerical model, Zhou and Yan [16], created a parametric study that examined the influence of factors such as interaction degree, force ratio (depending on the longitudinal reinforcement present in the concrete slab), and I-section slenderness parameters under LDB. Zhou and Yan [16], discovered that the degree of shear connectivity has a minor impact on LDB strength and that the web slenderness parameter is the most important factor in LDB strength.

The LDB strength of SCC beams was also the subject of a numerical study by Rossi et al. [17]. As stated by Rossi et al. [17], the presence of web stiffeners in the quarter points of the span

(L) under the action of uniform negative moment is responsible for an average 16% increase in LDB strength. Moreover, Rossi et al. [17] stated the need for further investigation on the LDB behaviour of SCC beams as the influence of critical parameters has not been fully understood by the structural engineering research and design community. The previous numerical studies by Zhou and Yan [16] and Rossi et al. [17] revealed inconsistencies in the influence of critical parameters on LDB. It is evident from the literature that there is a grey area of research regarding the LDB behaviour of SCC beams due to the inconsistencies in the significant factors that govern the LDB capacity, which is a fact that has not been properly addressed in standard codes. In this context, the objective of this study is to introduce a realistic modelling approach for better understanding the behaviour of the LDB of SCC beams that would provide valuable insights into their behaviour and performance under different loading conditions, which can assist engineers in optimizing their design and ensuring safe and reliable use in real circumstances.

3. Experimental Program

This study refers to the experimental tests done by Tong et al. [12] which is one of the most recent experimental studies dealing with stability phenomena in SCC beams under the action of negative moment. A brief description of the experiment to the extent required for validation is given below.

A total of five composite beam specimens were tested under uniform negative bending. Four beams were equipped with no transverse stiffeners in-between the supports, denoted by B3.0-350-1, B4.2-350-1, B4.2-350-1-C and B4.2-400-1, whereas the beam denoted B4.2-400-1-S was equipped with 3 transverse stiffeners in between the supports with a spacing of 700 mm. Furthermore, web stiffeners were positioned at both ends in all five specimens, as shown in Figure 3, to prevent any instability developing in the cantilevered regions. When designing the experiment, magnitude of impact factors such as the lateral slenderness ratio (L/r_y), web height-thickness ratio ($(d-2t_f)/t_w$), and degree of shear connection on the ultimate bending moment of the SCC beams have been considered. The test specimens were labelled as BL–d-(M_2/M_1),where, 'B' indicates the beam section, 'L' indicates the unrestrained span of the beam, 'd' indicates the depth of the beam and (M_2/M_1) indicates the moment ratio. In the specimensB4.2-350-1-C and B4.2-350-1-S, C stands for complete combination (full shear connection), and S stands for the presence of transverse stiffeners, respectively.

However, for the FEM in the current study, two specimens (B4.2-350-1 and B4.2-350-1-C) were chosen. The test specimen B4.2-350-1 that can effectively validate the numerical model was primarily taken into consideration by the authors as it provides variation of lateral displacement and failure modes in addition to the Moment-Rotation curves provided in Tong et al. [12]. Furthermore, due to the prolong computational time requirement in simulations, only the test specimen B4.2-350-1-C was chosen as it shares many geometrical characteristics with the specimen B4.2-350-1, which only differs in the degree of shear connection. The specimen B4.2-350-1 is a partial shear connection composite specimen, with stud spacing (d_s) of 300 mm. The stud spacing of the specimen B4.2-350-1-C, which is a full shear connection composite specimen, is 150 mm (Table 1). To prevent the composite beam from lateral displacement,lateral bracings were equipped at both sides of the mid-span of the concrete slab and each support of the concrete slab.

Loadings were acted on the two ends of the specimens continuously till the specimens were damaged (Figure 4). The vertical and lateral displacements of the beam were measured using displacement transducers at the end support, one-half, and one-quarter points of the beam to investigate any distortional buckling of the entire beam. Furthermore, the rotation angle indictor was used to record the beam's end rotation angle, and the rotation capacity of the beam can then be defined using the Moment-Rotation curve [12].

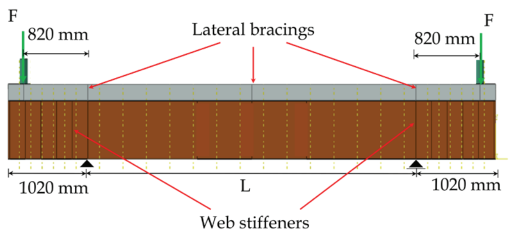

Figure 3 - Boundary Condition Adopted in the Experiment by Tong et al. [12]

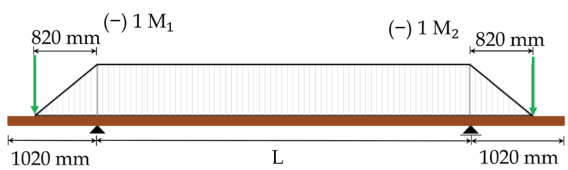

Figure 4 - Uniform Moment Configuration (M_2/M_1)

4. Finite Element Model

The FE software package ABAQUS was used in the present study to develop the numerical models. This software can be used to create elastic stability analyses as well as physical and geometric nonlinear analyses. The model's key information is discussed in the following subsections.

4.1 Geometric Model

Two composite beam specimens were modelled under uniform negative bending and the details of the cross section and geometric parameters of these two specimens are given in Figure 5 and Table 1, respectively.

The lateral bracings were modelled indirectly by applying boundary conditions which prevent lateral displacements at the same points on the beam as the lateral bracings were located in the tests. Due to the symmetrical geometry and loading, only half of the beams were modelled in the loading case (M_2/M_1) =1, while appropriate boundary conditions were applied on the plane of symmetry. Web stiffeners placed at cantilever ends were also incorporated in the model, as shown in Figure 6.

4.2 Element Type and Mesh

The developed numerical models adequately describe the geometry of the problem. Headed stud shear connectors were used to ensure the composite behaviour of the I-section and the concrete slab. Figure 7 depicts the Finite Elements that were used to develop the numerical model.

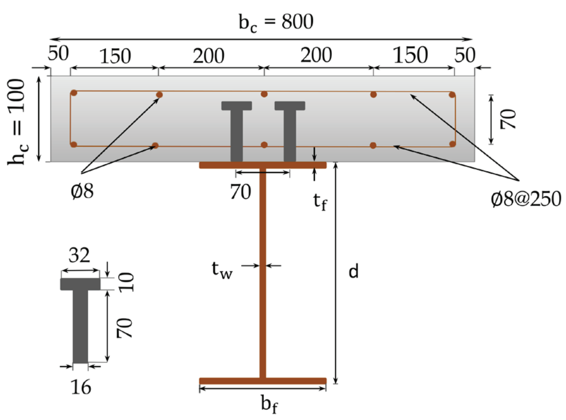

Figure 5 – Details of the Cross Section (All Dimensions are in mm)

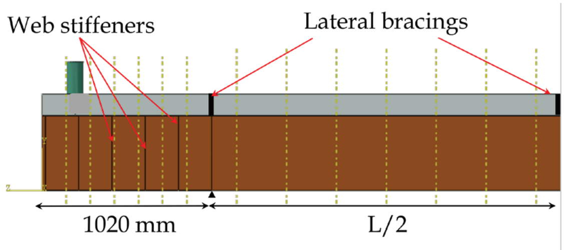

Figure 6 – Details of the Half Model

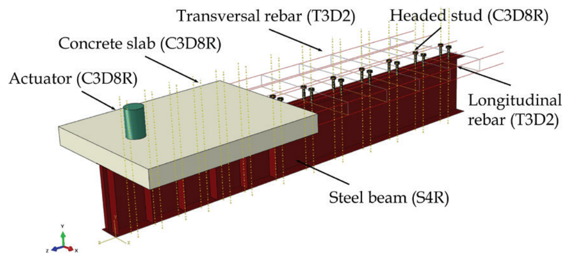

Figure 7 – Element Types Used in Numerical Model

The eight-node linear hexahedral solid elements with reduced integration and hourglass control were used to model the concrete slab, headed stud shear connectors, and actuator (C3D8R). Each node of the C3D8R element has 3 degrees of freedom (three translations).

Elements with reduced integration were chosen because they could reduce computer processing time. The shear connection modelling in a composite beam is probably the most complicated task due to the complex interaction between the studs and the concrete slab.

Sensitivity analysis which defined the optimum mesh configuration in the current study was done by measuring the rotation of the steel beam at half height of the web in support region and the reaction force was measured at the centre of actuator top surface. The I-beam discretised with S4R elements and concrete slab discretised with C3D8R elements show that the size of the 8 mm element provides good results with relatively low processing time (Figure 8). Table 2 shows the dimensions used in the discretization of each element, which can be seen in Figure 9.

Table 1 – Geometric Parameters of Test Specimens [12]

Test specimen number	L (mm)	d (mm)	b_f(mm)	t_f(mm)	t_w(mm)	d_s (mm)
B4.2–350-1	4200	350	125	8	6	300
B4.2–350-1-C	4200	350	125	8	6	150

Table 2 – Dimensions Used in Each Element's Discretization

Element	Element type	Element size (mm)
Concrete slab	C3D8R	8
Steel I-beam	S4R	8
Reinforcement bars	T3D2	10
Headed stud	C3D8R	4
Actuator	C3D8R	10

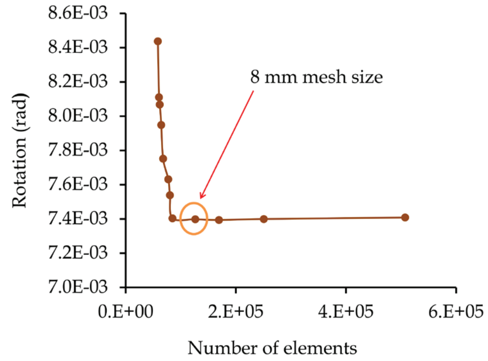

a) Steel beam

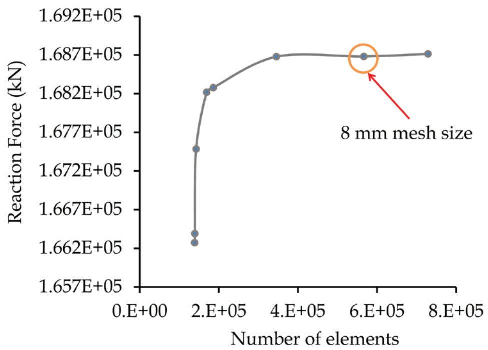

b) Concrete slab

Figure 8 – Mesh Convergence Test Results

4.3 Material Properties

The mechanical properties of the materials used for the development of numerical models are shown in Table 3.

4.3.1 Steel

The adopted constitutive relationship proposed by Earls [18] was used for the steel beam. The stress-strain relationship presented by Earls [18] is a quad-linear curve as shown in Figure 10(a)-(b). A bi-linear curve was employed to describe the stress-stain relationship for the rebar as in Figure 10(c). The model assigned to the headed stud shear connectors was the perfect elastic - plastic, as shown in Figure 10(d). The stress-strain response of steel was simulated by isotropic hardening model.

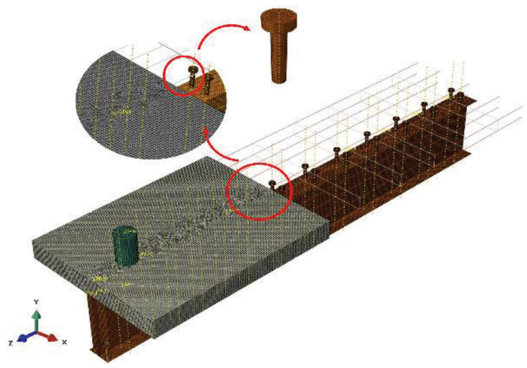

Figure 9 – Discretised Model

4.3.2 Concrete

The concrete material was represented by the Concrete Damage Plasticity (CDP) model. The CDP model is a criterion based on the models proposed by some authors (Hillerborg [19]; Lubliner [20]), and has been widely used in modeling concrete and other quasi-brittle materials. Based on the plasticity theory, the model considers three hypotheses: the initial yield surface determines when plastic deformation begins, the flow rule determines the direction of plastic deformation, and the softening/hardening rule defines how the surface flow evolves with plastic deformation [21].

The input parameters to characterize the plasticity are: dilation angle (ψ), eccentricity (ξ), the ratio of initial biaxial compressive yield stress to initial uniaxial compressive yield stress (σ_{b0}/σ_{c0}), the ratio of the second stress invariant on the tensile meridian to that on the compressive meridian (K_c), and the viscosity parameter that represents the relaxation (μ). Table 4 presents the values of these parameters used for the numerical model development [17], [22], [23]. The main failure mechanisms of the CDP model are tensile cracking and compression crushing of concrete. As a result, the flow surface evolution is governed by two hardening variables that cause rupture under tension and compression. The irreversible damage that occurs during the fracture process can be described using this damage model.

The variables that define material damage can be calculated using Eqs. (1) and (2) for concrete in compression and tension, respectively. This parameter has a value ranging from "0" (undamaged material) to "1" (totally damaged material).

$$d_c = 1 - (\sigma/f_c) \qquad \ldots (1)$$

$$d_t = 1 - (\sigma/f_t) \qquad \ldots (2)$$

Table 3 – Material Properties [12]

Element	E (GPa)	v	$f_{ck-cubic}$ (MPa)	f_y (MPa)	f_u(MPa)
Concrete slab	27.12	0.2	25.1	-	-
I-beam flange	205	0.3	-	403	522
I-beam web	207	0.3	-	362	489
Reinforcement bars	211	0.3	-	530	657
Headed stud	206	0.3	-	235	-

Note: E is the Young's modulus, v is the Poisson's ratio, $f_{ck-cubic}$ is the characteristic cubic strength, f_y is the yield stress and f_u is the ultimate stress.

Table 4 – CDP Input Parameters

Parameter	Value	Reference
Ψ (°)	36.0	[17], [22], [23]
ξ	0.1	(Default)
σ_{b0}/σ_{c0}	1.16	(Default)
K_c	0.667	(Default)
μ (s^{-1})	0.001	[17], [22], [23]

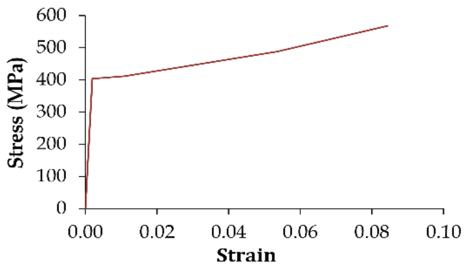

a) Steel beam flange

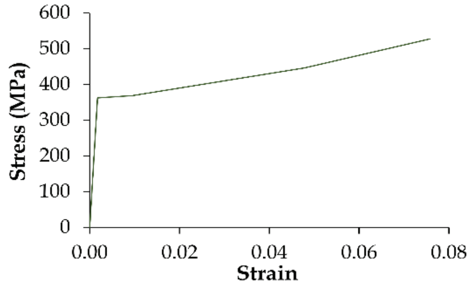

b) Steel beam web

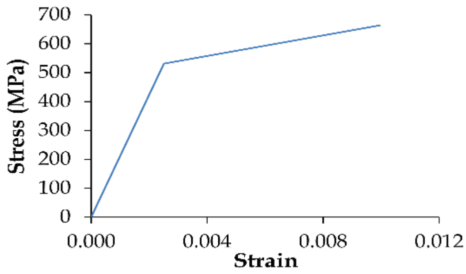

c) Reinforcement bar

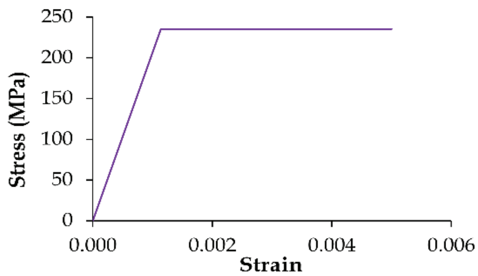

d) Headed shear stud

Figure 10 – Stress-Strain Relationship of Steel

The concrete material stress–strain relationship was calibrated according to the values obtained from the concrete cube tests. The stress–strain law proposed by Carreira and Chu [24], Eqs. (3) -(4), was used to represent the behaviour of concrete in compression. For the representation of the concrete behaviour in tension, Carreira and Chu [25] proposal represented by Eq. (5) was used. Figure 11 represents the stress–strain relationship used to represent the behaviour of concrete in compression and tension. For modelling the concrete behaviour, the damaged plasticity model was chosen over the smeared cracked model as it models concrete behaviour more realistically than the companion model (smeared crack model). However, it is computationally more expensive. Because of its numerical efficiency when full inelastic response must be captured, CDP model was chosen in the current study [5].

$$\frac{\sigma}{f_c} = \frac{\beta_c(\varepsilon/\varepsilon_c)}{\beta_c - 1 + (\varepsilon/\varepsilon_c)^{\beta_c}} \quad \dots (3)$$

$$\beta_c = \left(\frac{f_c}{32.4}\right)^3 + 1.55\ (MPa) \quad \dots (4)$$

$$\frac{\sigma}{f_t} = \frac{\beta_c(\varepsilon/\varepsilon_t)}{\beta_c - 1 + (\varepsilon/\varepsilon_t)^{\beta_c}} \quad \dots (5)$$

where f_c is the compressive strength of concrete, f_t is the tensile strength of concrete, ε_c is the compressive strain and the ε_t is the tensile strain value at peak stress and $\beta_c$is a material parameter that depends on the shape of the stress-strain diagram.

For the definition of the elastic modulus E_c (Eq. (6)), the tensile strength of concrete f_t (Eq. (7)) and the compressive strain ε_c in the concrete at the peak stress (Eq. (8)), the definitions presented in Eurocode 2 [26] were adopted.

$$E_c = 22\left(\frac{f_c}{10}\right)^{0.3} \ (MPa) \quad \ldots (6)$$

$$f_t = 0.3 f_c^{2/3} (MPa) \quad \ldots (7)$$

$$\varepsilon_c = 0.7 f_c^{0.31} \leq 2.8\% \quad \ldots (8)$$

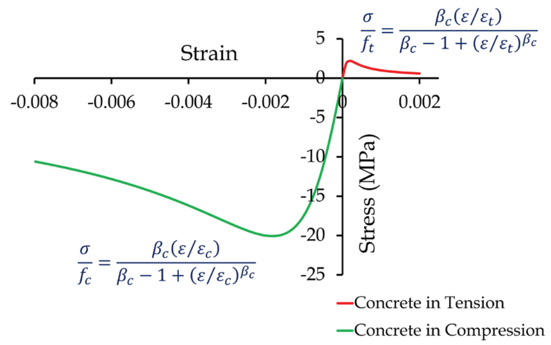

Figure 11 – Stress-Strain Relationships of Concrete

4.4. Contact Properties

The interaction between the constituent parts of the numerical model was performed using the interaction and constraint options available in ABAQUS. The model interaction details can be seen in Figure 12.

The interaction option Shell-to-Solid coupling was used over Tie constraint option available in ABAQUS to simulate the welded connection between the headed stud and the top flange of I-beam. In the case of using shell element (S4R) to model the steel beam and solid elements (C3D8R) to model the headed shear studs, using tie constraint option, seems to be less precise as the rotational degrees of freedom in shell element are not taking into account at the shear stud, steel I-beam interface. When using tie constraint to join shell and solid elements, nodes are tied together where surfaces are very close to each other and, in the case of shell edges, which is typically only along a line in the center of the thickness being represented. Shell-to-Solid coupling, on the other hand, considers the thickness of the shell even when it is joined to the solid along its edge. Instead of simply connecting local nodes, ABAQUS creates constraints that link the displacement and rotation of each shell node to the average displacement and rotation of the solid surface in its vicinity. This enables the distribution of forces and moments acting at the shell node to be translated to forces (no rotational degrees of freedom in solid element nodes) on the related set of coupling surface nodes in a self-equilibrating context.

The surface-to-surface interaction option was used to perform the interactions between the following surfaces: headed stud-concrete slab and concrete slab-steel beam. The "Hard" and "Penalty" options were used to define the normal and tangential behaviour between these contact surfaces. The friction coefficient was set to 0.4 [17].

For the interaction of reinforcement in the slab, the embedded element technique was employed. In ABAQUS, the embedded element technique is used to specify an element or group of elements that are embedded in a group of host elements. The perfect bond between the host elements and embedded elements will constrain the embedded nodes' degrees of freedom in translation. In the present case, the truss elements representing the reinforcement are the embedded region while the concrete slab is the host region.

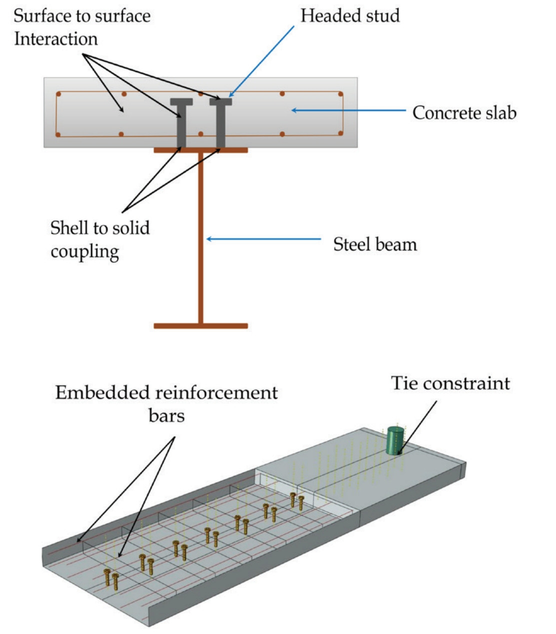

Figure 12 – Interactions Developed in Numerical Model

4.5 Boundary Conditions

The SCC beams are simply supported with lateral bracings in terms of boundary conditions (Figure 3). The lateral bracings simulate a composite floor with infinite stiffness in the slab plane (transversal stiffness). This situation prevents the composite beam from lateral displacement, which is similar to the restrictions developed by Tong et al. [12], and Zhou and Yan [16]. The lateral bracings were modeled indirectly by applying boundary conditions that prevent lateral displacements at the same points on the beam as the lateral bracings were located in the tests. According to the uniform negative moment distribution configuration (Figure 4), forces can be applied at one or both ends (cantilever) of the beam. In the internal span (L) between supports, the possible modes of instability (LDB or LB (local buckling)) that govern the strength of these elements are analyzed. The details of the boundary conditions developed in the numerical model can be seen in Figure 13.

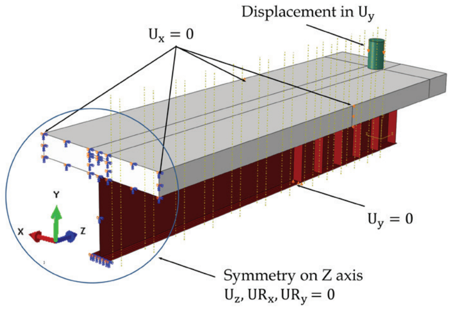

Figure 13 - Details of the Boundary Conditions Adopted in Numerical Model

4.6 Solver Method and Initial Imperfections

The buckle linear perturbation method was used to estimate the critical elastic stability load for the elastic stability analysis by obtaining eigenvalues and eigenvectors. The elastic stability load is calculated using this method by multiplying the first positive eigenvalue by the external load applied to the structure in its initial state. Importantly, this type of analysis does not take into account any structural imperfection. Following that, the geometric nonlinear analysis is performed, taking into account the initial geometric imperfections. At the beginning of this analysis, the structure shape from the elastic stability analysis was used which is normalized to the initial imperfection value.

According to the Chinese Specification for Steel Work, the maximum amplitude of geometric imperfections in the steel bottom flange is limited to 1/1000 of the steel beam's length or 5 mm, whichever is smaller, as shown in Figure 14 [7]. Thus, the geometric imperfection with amplitude of L/1000 was implemented. The residual stresses were considered in the models because they are responsible for reducing the resistance of structural elements in the inelastic buckling regime, which occur due to premature flow of steel [27]. To consider residual stresses, stress distribution model proposed by Galambos and Ketter [28]was used (Figure 15). The sensitivity analysis on initial imperfections conducted by Rossi et al. [29] revealed that the initial imperfections used herein provide greater accuracy in estimating the LDB strength of SCC beams.

The geometric nonlinearity problem was solved using the Static Riks method. This method, also known as the modified Riks algorithm, can capture any possible local instability [5], [29], [30].

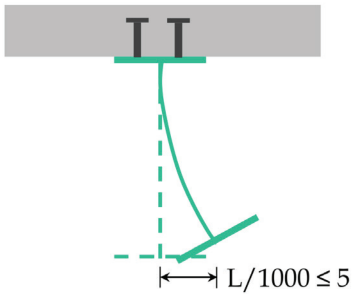

Figure 14 - Initial Geometric Imperfection used in FEM

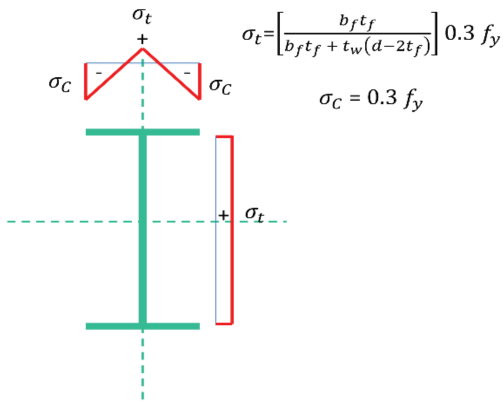

Figure 15 - Galambos and Ketter Residual Stress Pattern [28] used in FEM

5. Validation of Numerical Analysis with Experimental Data

The accuracy of the simulation results was verified by comparing with the results of experimental tests performed on uniform moment configuration (M_2/M_1=1) by Tong et al. [12].

The rotations of the beams were measured at half height of the web near the support region, as stated by Tong et al. [12]. However, there is insufficient experimental data to ensure the exact procedure and location of measuring rotations. Hence, the rotation measurements of FE models were obtained at three different locations, as shown in Figure 16.

The comparison focuses on aspects such as Moment–Rotation curve (Figure 17), lateral displacement of the bottom flange along the axial direction (Figure 18), failure mode comparison between the numerical model and the experimental test specimen (Figure 19) andmoment capacity of beams (Table 5). The influence of residual stresses on ultimate moment capacity(M_u) is shown in Figure 20, which emphasizes the importance of incorporating residual stresses in FEM.

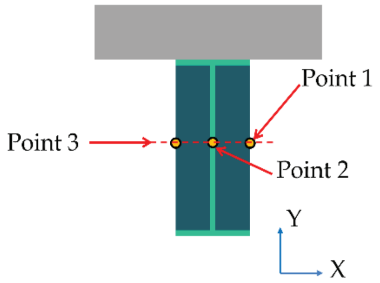

Figure 16 – Locations for Rotation Measurements in FEM

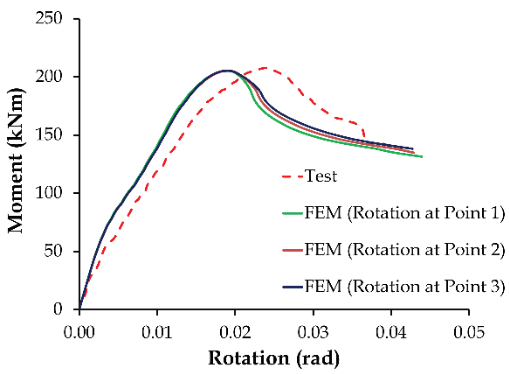

a) B4.2–350-1

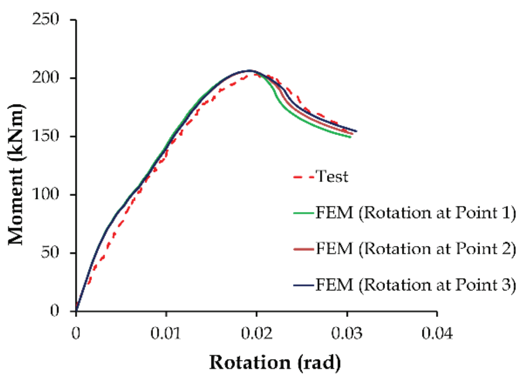

b) B4.2–350-1-C

Figure 17 - Test vs. FEM Results

The results of the numerical models and the experimental tests were found to be in agreement as shown in Table 5. The subtle difference in the LDB ultimate moment between Tong et al. [12] physical models and the numerical models was less than 2%. It was observed that there is a slight deviation in rotation of the Moment-Rotation curve of the beam with partial shear connectivity (B4.2-350-1) (Figure 17(a)). Therefore, further investigation would be required in this scenario. However, the beam with full shear connectivity (B4.2-350-1-C) provides better agreement of Moment-Rotation curves in Test and FEM in terms of ultimate moment and rotation (Figure 17(b)). Therefore, the numerical models developed here in demonstrated the ability to reasonably accurately represent the LDB strength.

The typical lateral displacement of the bottom flange along the axial direction is shown in Figure 18, where M_u represents the ultimate bending moment of SCC beam.

The lateral displacement of the bottom flange of FEM near the support region was found to be less than the experimental value. This could be due to the placement of web stiffeners near the support region on either sides. However, sufficient information which is necessary to confirm the precise location of web stiffeners in the support region has not been provided by Tong et al. [12]. Moreover, the maximum lateral displacement of FEM was observed to be at the mid span of B4.2–350-1, which agrees well with the experimental value. The relative error between the maximum lateral displacement between the Tong et al. [12] physical model and FEM was found to be 2%. This is due to the absence of the restraint that would result from the presence of web stiffeners between the supports.

The failure modes observed between experimental test specimens and the numerical model were found to be in good agreement in representing the LDB phenomenon, as shown in Figure 19. Therefore, the numerical models are validated given by the conformity of the results and can be used for the development of the parametric study in future.

The LDB behaviour in SCC beams is considered to be more sensitive to residual stress distribution patterns, as shown in Figure 20, and it has been proven that the initial imperfections chosen for the development of post buckling numerical analyses have a significant impact on the LDB strength of SCC beams which cannot be neglected.

Table 5 – Comparison of Test vs Numerical Results

Test specimen	M_{Test} (kNm)	M_{FEM} (kNm)	M_{FEM}/M_{Test}	Error (%)
B4.2–350-1	206.9	205.3	0.992	0.8
B4.2–350-1-C	203.7	206.1	1.017	1.2

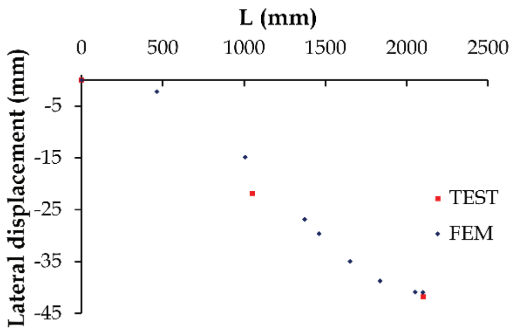

Figure 18 - Lateral Displacement of the Bottom Flange Along the Axial Direction at M_u (B4.2–350-1)

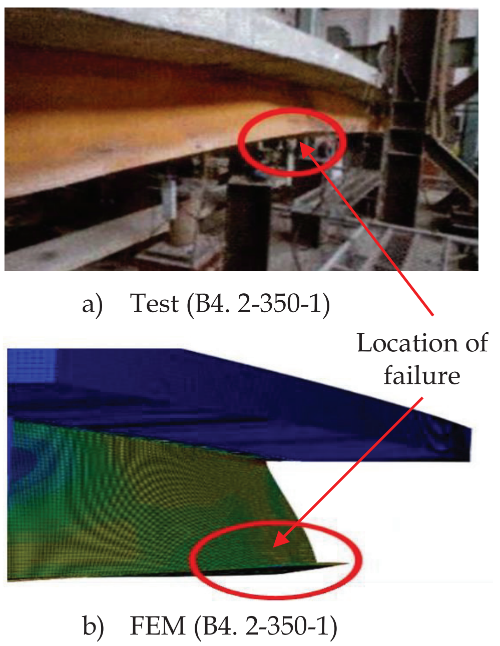

Figure 19 - Comparison of Failure Mode Between FEA and Experiment in Specimen (B4. 2-350-1)

6. Conclusions

This study focused on developing 3-Dimensional FE models to study the LDB resistance in SCC beams. Through this study,

- It was found that the implementation of contact and interaction features which are used herein provided more realistic behaviour of SCC beam in numerical modelling. However, further verification would be required to address the issue in initial bending stiffness.

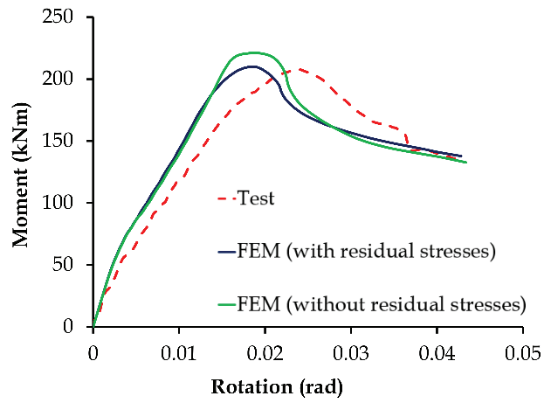

a) B4.2–350-1

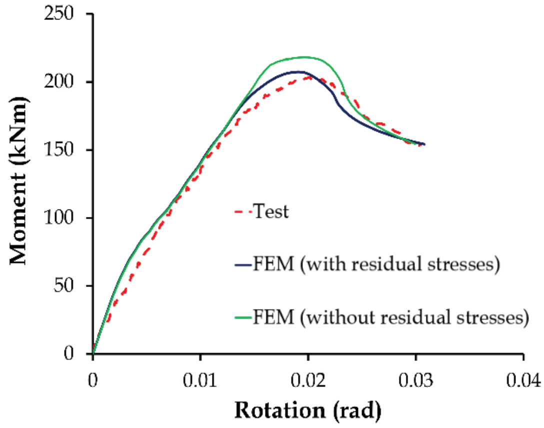

b) B4.2–350-1-C

Figure 20 – Effect of Residual Stresses on M_u

- The inclusion of physical imperfections in FE models was found to be critical as they are responsible for reducing the resistance of structural elements.

- The location of distortional buckling in steel beam flange was captured accurately by the FE analysis.

- The difference in the LDB ultimate moment between referred experimental models and the numerical models was less than 2%.

Therefore, the proposed 3-Dimensional FE model provides the framework for developing more realistic models to predict the LDB phenomenon. The authors suggest further investigations to decide on an optimal web stiffener configuration that minimizes the LDB effect in SCC beams.

Acknowledgement

Authors wish to acknowledge the licensed applications of the ABAQUS package facilitated by the Finite Element Analysis and Simulation Center, Rubber Research Institute of Sri Lanka, Ratmalana.

References

1. Ding, F. X, Liu, J., Liu, X. M., Guo, F. Q., Jiang, L. Z., "Flexural Stiffness of Steel-Concrete Composite Beam Under Positive Moment", *Steel and Composite Structures,* Vol. 20, No. 6, 2016, pp. 1369-1389.

2. de Lima Araújo, D., Sales, M. W. R., de Paulo, S. M., de Cresce El, A. L. H., "Headed Steel Stud Connectors for Composite Steel Beams with Precast Hollow-Core Slabs with Structural Topping", *Engineering Structures,* Vol. 107, 2016, pp. 135-150.

3. Adluri, S., *Structural Steel Design Composite Beams,* 2005, 13 p.

4. Loqman, N., Safiee, N.A., Bakar, N.A, Nasir, N. A. M., "Structural Behavior of Steel-Concrete Composite Beam using Bolted Shear Connectors :A Review", *MATEC Web of Conferences,* 2018.

5. Vasdravellis, G., Uy, B., Tan, E. L., Kirkland, K., "The Effects of Axial Tension on the Hogging-Moment Regions of Composite Beams", *Journal of Constructional Steel Research*, 2012, pp. 20-23.

6. Rossi, A., de Souza, A. C., Nicoletti, R. S., Martins, C. H., "Lateral Distortional Buckling in Steel Concrete Composite Beams: A Review", *Structures,* Vol. 27, 2020, pp. 1299-1312.

7. Chen, S., Jia, Y., "Numerical Investigation of Inelastic Buckling of Steel–Concrete Composite Beams Prestressed with External Tendons", *Thin-Walled Structures,* Vol.48, 2010, pp. 233–242.

8. Pezeshky, P., Mohareb, M., "Distortional Lateral Torsional Buckling of Beam-Columns including Pre-Buckling Deformation Effects", *Computers & Structures,* Vol.209, 2018, pp. 93-116.

9. Tohidi, S., Sharif, Y., "Neural Networks for Inelastic Distortional Buckling Capacity Assessment of Steel I-Beams", *Thin-Walled Structures*, 2015, pp. 359-371.

10. Dias, J. V. F., Oliveira, J. P. S., Calenzani, A. F. G., Fakury, R. H., "Elastic Critical Moment of Lateral-Distortional Buckling of Steel-Concrete Composite Beams under Uniform Hogging Moment", *International Journal of Structural Stability and Dynamics,* Vol. 19, No. 07, 2019.

11. Abdollahi, A., "Numerical Strategies in the Application of the FEM to RC Structures—I", *Computers & Structures,* Vol. 58, No. 6, 1996, pp. 1171-1182.

12. Tong, L., Liu, Y., Sun, B., Chen, Y., Zhou, F., Tian, H., Sun, X., "Experimental Investigation on Mechanical Behavior of Steel-Concrete Composite Beams under Negative Bending", *Journal of Building Structures,* Vol. 35, 2014.

13. Bradford, M. A., Kemp, A. R., Buckling in Continuous Composite Beams", *Progress in Structural Engineering and Materials*, 2000, pp. 169-178.

14. Chen, S., Wang, X., "Finite Element Analysis of Distortional Lateral Buckling of Continuous Composite Beams with Transverse Web Stiffeners", *Advances in Structural Engineering,* Vol. 15, 2012, pp. 1607–16.

15. Liu, Y., Sun, B., "Experimental Investigation and Finite Element Analysis for Mechanical Behavior of Steel-Concrete Composite Beams under Negative Bending", *International Conference on Mechanics and Civil Engineering,* Shanghai, China, Atlantis Press, 2014.

16. Zhou, W. B., Yan, W. J., "Refined Nonlinear Finite Element Modelling Towards Ultimate Bending Moment Calculation for Concrete Composite Beams under Negative Moment", *Thin-Walled Structures,* Vol.116, 2017, pp. 201-211.

17. Rossi, A., de Souza, A. C., Nicoletti, R. S., Martins, C. H. "Numerical Assesment of Lateral Distortional Buckling in Steel-Concrete Composite Beams." *Journal of Constructional Steel Research,* Vol. 172, 2020.

18. Earls, C. J., "Effects of Material Property Stratification and Residual Stresses on Single Angle Flexural Ductility", *Journal of Constructional Steel Research,* Vol.51, 1999, pp. 147–175.

19. Hillerborg, A., Modéer, M., Petersson, P. E., "Analysis of Crack Formation and Crack Growth in Concrete by Means of Fracture Mechanics and Finite Elements", *Cement and Concrete Research,* Vol. 6, 1976, pp. 773–781.

20. Lubliner, J., Oliver, J., Oller, S., Onate, E., "A Plastic Damage Model for Concrete", *Int. J. Solids Structures,* Vol. 25, 1998, pp. 299-326.

21. Yu, T., Teng, J. G., Wong, Y. L., Dong, S. L., "Finite Element Modeling of Confined Concrete-I : Drucker – Prager Type Plasticity Model", *Eng. Struct.,* Vol.32, 2010, pp. 665-679.

22. Rossi, A., de Souza, A. C., Nicoletti, R. S., Martins, C. H., "Stability Behavior of Steel–

Concrete Composite Beams Subjected to Hogging Moment", *Thin-Walled Struct.,* Vol.167, 2021.

23. de Olivera, V. M., Rossi, A., Ferreira, F. P. V., Martins, C. H., ''Stability Behaviour of Steel-Concrete Composite Beams Subjected to Hogging Moment'', *Thin-Walled Structures, February, 2022.*

24. Carreira, D. J., Chu, K. H., "Stress-Strain Relationship for Reinforcement Concrete in Compression", *ACI Journal*, 1985.

25. Carreira, D. J., and Chu, K. H., "Stress-Strain Relationship for Reinforced Concrete in Tension", *ACI Journal*, 1986.

26. *EC2 Eurocode 2, Design of Concrete Structures Part1-1, General Rules and Rules for Buildings.* London, UK: British Standards Institution, 2004.

27. Szalai, J., Papp, F., "A New Residual Stress Distribution for Hot-Rolled I-Shaped Sections", *J.Constr. Steel Res.,* Vol. 61, 2005, pp. 845-861.

28. Galambos, T. V., Ketter, R. L., "Columns under Combined Bending and Thrust", *Journal of Engineering Mechanics,* Vol. 85, 1959, pp. 1-30.

29. Rossi, A., de Souza, A. C., Nicoletti, R. S., Martins, C. H., "The Influence of Structural and Geometric Imperfections on the LDB Strength of Steel–Concrete Composite Beams", *Thin-Walled Structures,* Vol.162, 2021.

30. Shamass, R., Cashell, K. A., "Behaviour of Composite Beams Made using High Strength Steel", *Structures,* Vol. 12, 2017, pp. 88-101.